## EDGE ARTICLE

Check for updates

# Integration of plasma and electrocatalysis to synthesize cyclohexanone oxime under ambient conditions using air as a nitrogen source†

Shunhan Jia, [ID] [ab] Xingxing Tan,[a] Limin Wu,[ab] Xiaodong Ma,[a] Libing Zhang,[ab] Jiaqi Feng,[a] Liang Xu,[ac] Xinning Song, [ID] [ab] Qinggong Zhu, [ID] [ab] Xinchen Kang, [ID] [ab] Xiaofu Sun [ID] *[ab] and Buxing Han [ID] *[abd]

Direct fixation of $N_2$ to N-containing value-added chemicals is a promising pathway for sustainable chemical manufacturing. There is extensive demand for cyclohexanone oxime because it is the essential feedstock of Nylon 6. Currently, cyclohexanone oxime is synthesized under harsh conditions that consume a considerable amount of energy. Herein, we report a novel approach to synthesize cyclohexanone oxime by *in situ* $NO_3^-$ generation from air under ambient conditions. This process was carried out through an integrated strategy including plasma-assisted air-to-$NO_x$ and co-electrolysis of $NO_x$ and cyclohexanone. A high rate of cyclohexanone oxime formation at 20.1 mg $h^{-1}$ $cm^{-2}$ and a corresponding faradaic efficiency (FE) of 51.4% was achieved over a $Cu/TiO_2$ catalyst, and the selectivity of cyclohexanone oxime was >99.9% on the basis of cyclohexanone. The C–N bond formation mechanism was examined by *in situ* experiments and theoretical calculations, which showed that cyclohexanone oxime forms through the reaction between an $NH_2OH$ intermediate and cyclohexanone.

## Introduction

Dinitrogen ($N_2$) constitutes approximately 80% of the air, and is an inexhaustible nitrogen source that can be used to produce N-containing chemicals with a wide range of applications.[1,2] However, because of the ultra-inert N≡N triple bonds, the kinetics are sluggish and the thermodynamics are limited for the conversion of $N_2$.[3–5] Over the past few decades, researchers were mainly focused on the fixation of $N_2$ to $NH_3$ as a feedstock that would be further processed into various organonitrogen chemicals through reductive amination, oxidative cyanation, and ammoxidation.[6–8] Industrial $NH_3$ production through the traditional Haber–Bosch process consumes large amounts of energy and emits high levels of $CO_2$, and therefore cannot meet the demands for carbon neutrality or sustainability goals.[9–11] As an alternative route, the direct utilization of $N_2$ to construct C–N bonds under mild conditions is a promising strategy for the production of value-added chemicals and the decoupling of chemical manufacturing from fossil fuel energy, but it is a challenge.[12–14]

There is great interest in the use of the electrochemical $N_2$ reduction reaction (NRR) to produce $NH_3$ because of the utilization of renewable electricity and protons directly from water.[15–17] The electrochemical construction of the C–N bond *via* the coupling of $CO_2$ and $N_2$ has also been considered to produce some organonitrogen chemicals, such as urea.[18,19] However, the reported reactions are very limited, and they are hindered by low reactivity and selectivity due to low $N_2$ solubility, difficult $N_2$ activation, and undesired hydrogen evolution reaction (HER).

Based on the occurrence of lightning in nature, air plasma oxidation offers an effective method for $N_2$ activation. Air can be converted into reactive $NO_x$ or $NO_x^-$, which can be used as a N source in electrolysis.[20,21] The C–N coupling would be achieved by the *in situ* generation of nucleophilic N-containing intermediates followed by their coupling with carbon substrates or intermediates as the electrophile.[22,23]

Cyclohexanone oxime is the essential feedstock of Nylon 6, with worldwide annual demand of approximately 10 million tons and an approximate global market size of USD 25 billion, and is currently produced through the coupling between

*[a]Beijing National Laboratory for Molecular Sciences, CAS Laboratory of Colloid and Interface and Thermodynamics, CAS Research/Education Center for Excellence in Molecular Sciences, Center for Carbon Neutral Chemistry, Institute of Chemistry, Chinese Academy of Sciences, Beijing 100190, China. E-mail: sunxiaofu@iccas.ac. cn; hanbx@iccas.ac.cn*

*[b]School of Chemical Sciences, University of Chinese Academy of Sciences, Beijing 100049, China*

*[c]State Key Laboratory of Organic-Inorganic Composites, College of Chemical Engineering, Beijing University of Chemical Technology, Beijing 100029, China*

*[d]Shanghai Key Laboratory of Green Chemistry and Chemical Processes, School of Chemistry and Molecular Engineering, East China Normal University, Shanghai 200062, China*

cyclohexanone and $NH_2OH$ intermediates from unsustainable $(NH_3OH)(NH_4)SO_4$ (Scheme 1).[24–26] Therefore, optimization of N sources for $NH_2OH$ intermediates is urgently needed for cyclohexanone oxime production. Researchers have recently explored the synthesis of cyclohexanone oxime using *in situ*-generated $H_2O_2$ to produce $NH_2OH$ intermediates from $NH_3$.[8] Furthermore, the direct use of $N_2$ *via* air plasma oxidation integrated with electroreduction may result in the formation of cyclohexanone oxime under ambient conditions.

Herein, we report the first work to efficiently synthesize cyclohexanone oxime using air as the nitrogen source by combining plasma-assisted air-to-$NO_x$ and co-electrolysis of $NO_x$ and cyclohexanone. A faradaic efficiency (FE) of 51.4% was achieved for cyclohexanone oxime with a corresponding formation rate of 20.1 mg $h^{-1}$ $cm^{-2}$ and remarkable catalyst ($Cu/TiO_2$) recyclability. The superior performance can be attributed to Cu sites supported on $TiO_2$ with a stable oxidation state. In addition, the reaction pathway was studied based on *in situ* experiments and theoretical calculations.

## Results and discussion

As shown in Fig. 1A, as a proof-of-concept, we synthesized cyclohexanone oxime through the coupling of plasma air activation and $NO_x$ electroreduction with cyclohexanone (Fig. S1†). A model air mixture of $N_2/O_2$ (v/v = 4/1) was used as the nitrogen source. The reaction between $N_2$ and $O_2$ activated by plasma produced $NO_x$, which was absorbed by 1 mol $L^{-1}$ NaOH aqueous solution, and the as-obtained solution was directly used as an electrolyte for further electrosynthesis (Fig. S2 and S3†). This process holds the potential to block the interference of trace $H_2O$ and $CO_2$ from real air. The concentration of $NO_3^-$ and $NO_2^-$ was quantified by UV-Vis spectroscopy measurements (Fig. S4†). Fig. 1B shows that the yield of $NO_x$ linearly increased over the plasma activation time, in which the concentration of $NO_2^-$ was approximately 2 times that of $NO_3^-$. A high total $NO_x$ concentration of approximately 1 mol $L^{-1}$ was achieved after 400 min of plasma activation.

In the following electrosynthesis process, the electroreduction of $NO_3^-$ with cyclohexanone was initially verified as a model reaction in a flow cell with 1 mol $L^{-1}$ NaNO$_3$ and 50 mmol $L^{-1}$ cyclohexanone aqueous solution as the catholyte, and 1 mol $L^{-1}$ NaOH as the anolyte. Copper-based catalysts were selected due to their exceptional performance in nitrate reduction, as described in recent reports.[27–31] $Cu/TiO_2$ catalysts loaded onto porous carbon paper served as the cathode, and Ni foam was used as the anode.

The obtained catalysts contained 0.3, 0.6, and 0.9 wt% Cu, as determined by inductively coupled plasma optical emission spectroscopy (ICP-OES). We denoted these catalysts as 0.3% Cu/$TiO_2$, 0.6% Cu/$TiO_2$, and 0.9% Cu/$TiO_2$ for clarity. $H_2$ was the only gas product, and cyclohexanone oxime was the only organic product during electrolysis quantified by gas chromatography (GC). Colorimetric methods were used to study the aqueous byproducts, including $NO_2^-$ and $NH_3$ (Fig. S4 and S5†). We also identified cyclohexanone oxime *via* GC-mass spectrometry (GC-MS) and nuclear magnetic resonance (NMR) (Fig. S6–S10†). As shown in Fig. 1C, the molecular weight of 113.08354 provided by high-resolution GC-MS indicated that the molecular formula of the product is $C_6H_{11}NO$.

Using model air with $^{15}N_2$ gas and Na$^{15}$NO$_3$ as the reactant, the molecular ion peak of the product at 114.08057 and 114.08041 matched the calculated weight of 114.08055 for $C_6H_{11}^{15}NO$, which verified that the origin of nitrogen in cyclohexanone oxime was $NO_3^-$ *in situ* generated from air. Moreover, all the peaks in the $^1H$ NMR, $^{13}C$ NMR, and $^{15}N$ NMR (conducted with the $^{15}N$-labeled product) spectra were well matched with the standard samples (Fig. 1D and S9†). These results confirmed the formation of cyclohexanone oxime, with $NO_3^-$ as the nitrogen source.

Fig. 2A displays the linear sweep voltammetry (LSV) results for 0.6% Cu/$TiO_2$ in electrolyte with and without NaNO$_3$ plus cyclohexanone substrates. After the addition of the substrates, the sharpness of the increase in the current density ($j$) was greater than that of the initial NaOH electrolyte, which demonstrated that the electrosynthesis of cyclohexanone was more kinetically favorable than the HER. Electrochemical performance tests were carried out in the range of −1.0 V to −2.0 V *versus* Ag/AgCl, and the electrochemical performance of cyclohexanone oxime formation on Cu/$TiO_2$ is shown in Fig. 2B and C. The reactions under all the applied potentials presented a combined FE of approximately 100% for all products. A maximum cyclohexanone oxime FE of 50.0% and a corresponding formation rate of 20.1 mg $h^{-1}$ $cm^{-2}$ was achieved at −1.8 V over 0.6% Cu/$TiO_2$.

At low potentials, $NO_2^-$ was the main byproduct, which could be attributed to the hindered reductive hydrogenation of $NO_3^-$. Once the potential increased so that it was more negative than −1.8 V, the enhancement of the HER and the further electroreduction of $NH_2OH$ intermediates led to a decrease in the selectivity for cyclohexanone oxime (Fig. S11†). Intriguingly, the byproducts generated during the electrolysis process, specifically $NH_3$ and $H_2$, hold significant value as chemicals with substantial potential for further utilization. Under optimal conditions, the FE of $NH_3$ and $H_2$ were 21.6% and 16.4%, respectively. Similar trends were found for the Cu/$TiO_2$ catalysts with various Cu loadings. In addition, as shown in Fig. 2D, the
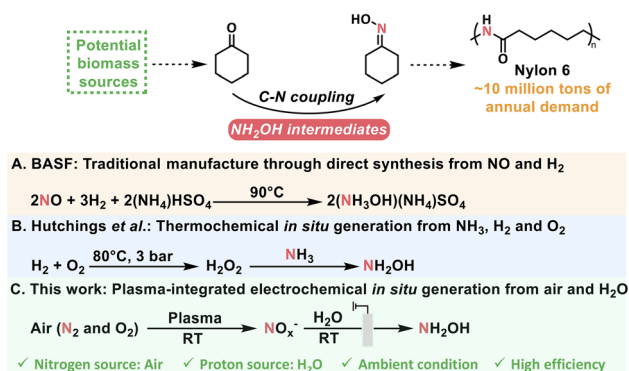


**Scheme 1** Schematic diagram of different production routes for cyclohexanone oxime.
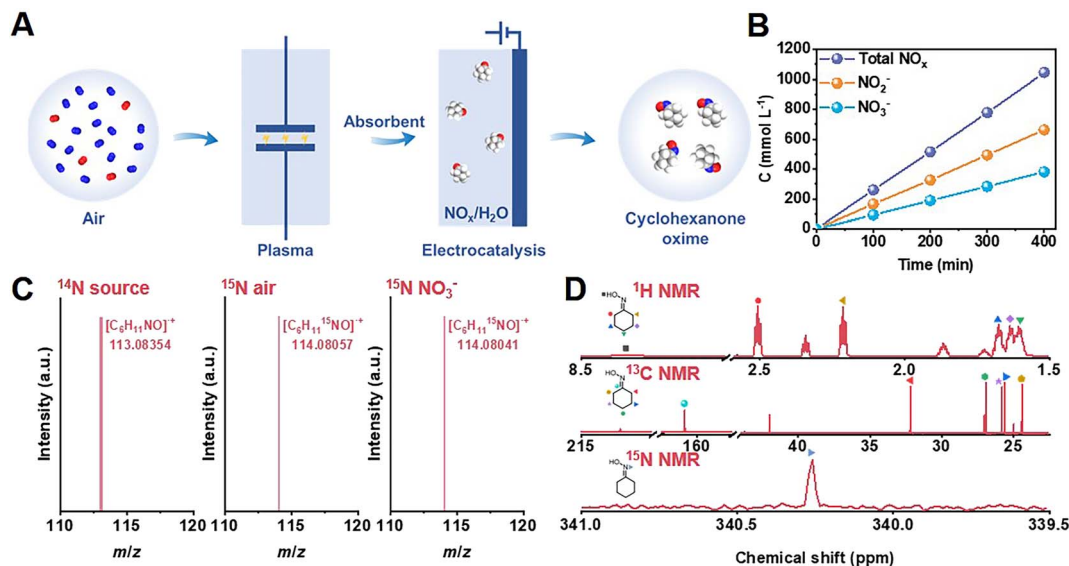
**Fig. 1** The integration system for cyclohexanone oxime synthesis. (A) Schematic illustration of the synthesis of cyclohexanone oxime with air as nitrogen source. (B) The concentration of $NO_x^-$ species under air activation. (C) GC-MS and (D) $^1H$ NMR, $^{13}C$ NMR, and $^{15}N$ NMR detection of cyclohexanone oxime.

corresponding chronoamperometry curve of 0.6% Cu/TiO$_2$ catalysts at −0.8 V remained stable during electrosynthesis.

We further studied the influence of substrate concentrations on the electrochemical performance by varying the molar concentrations of cyclohexanone and NaNO$_3$ in the electrolytes at the applied potential of −1.8 V vs. Ag/AgCl (Fig. S12†). This indicated that a higher cyclohexanone and NO$_3^-$ concentration promoted the formation of cyclohexanone oxime. However,

when the concentration of cyclohexanone was greater than 50 mmol L$^{-1}$, there was a significant decrease in the cyclohexanone oxime FE and formation rate due to the phase separation in the catholyte. The increase in the NO$_3^-$ concentration up to 2 mol L$^{-1}$ strengthened the side reaction of NH$_3$ formation, which was unsuitable for the formation of NH$_2$OH intermediates and cyclohexanone oxime. Consequently, the optimized substrate concentration was found to be 50 mmol L$^{-1}$
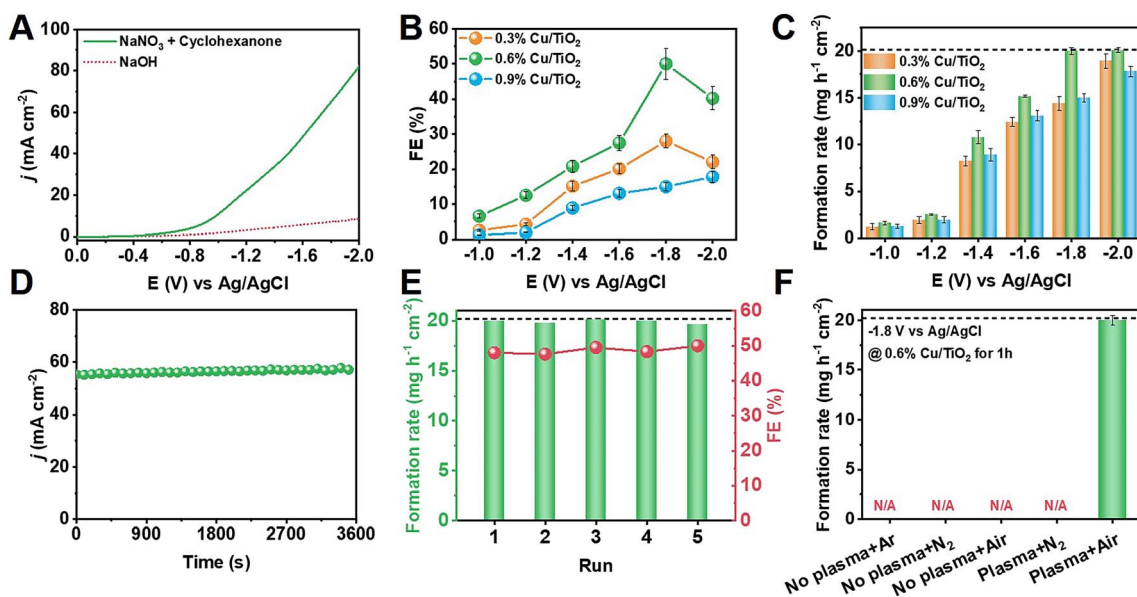


**Fig. 2** Electrochemistry study of cyclohexanone synthesis. (A) LSV curves of 0.6% Cu/TiO$_2$ catalysts in different electrolyte. Potential-dependent (B) FE and (C) formation rate of cyclohexanone oxime production on different Cu-loaded TiO$_2$ catalysts. (D) Chronoamperometry curves of 0.6% Cu/TiO$_2$ under optimal conditions for cyclohexanone oxime synthesis. (E) Recyclability of 0.6% Cu/TiO$_2$ electrocatalysts. (The dotted line shows the formation rate of cyclohexanone at 100% conversion.) (F) The formation rate of cyclohexanone oxime with different gas feed and plasma conditions.

cyclohexanone and 1 mol L$^{-1}$ NaNO$_3$ for cyclohexanone oxime production.

The TiO$_2$ support played a crucial role in the improvement of cyclohexanone oxime formation. Fig. S13† shows that the catalytic performance of the bulk TiO$_2$ was very poor. For comparison, carbon black was also used as a support for Cu loading, but the as-prepared Cu/carbon black catalyst exhibited a maximum cyclohexanone oxime FE of only 8.4% with a formation rate of 2.5 mg h$^{-1}$ cm$^{-2}$. Therefore, the optimized catalytic activity could be ascribed to the cooperation between Cu and the TiO$_2$ support.

The stability of the 0.6% Cu/TiO$_2$ catalyst was also studied at −1.8 V. Fig. 2E shows that there was no notable change in the cyclohexanone oxime FE or formation rate during 5 successive cycles, which was indicative of prominent recyclability and is important for practical applications.

After establishing the baseline of NO$_3^-$ electrolysis activity, NO$_x$ obtained from plasma air activation was fed together with cyclohexanone in the electrosynthesis process. Fig. 2F shows that the integrated system provided cyclohexanone oxime at a formation rate of 20.1 mg h$^{-1}$ cm$^{-2}$ using air as the nitrogen source. No cyclohexanone oxime was detected in the absence of either plasma, N$_2$, or O$_2$, indicating the necessity of air as the nitrogen source under plasma oxidation for cyclohexanone oxime production. It was therefore concluded that the two-step integration of plasma air activation with electrocatalytic reduction is practically feasible for highly efficient and selective nitrogen synthesis of cyclohexanone oxime under ambient conditions.

Structural and morphological measurements clarified that Cu nanoparticles were uniformly loaded on TiO$_2$ in the Cu/TiO$_2$ catalysts (Fig. S14–S22†). *In situ* X-ray absorption near-edge spectroscopy (XANES) was conducted to further investigate the electronic structure of the catalysts during cyclohexanone oxime synthesis. Fig. 3A shows that an initial 0.6% Cu/TiO$_2$ catalyst exhibited an absorption edge between that of Cu foil and Cu$_2$O samples, indicating that the oxidation state of Cu was between 0 and +1. We further acquired the Cu average oxidation state as a function of the Cu K-edge energy shift, and the value was 0.42 during the *in situ* measurements (Fig. 3B). The value did not change over electrolysis time, indicating the excellent stability of the Cu active sites during electrolysis. The results indicated that a stable slightly positive oxidation state for Cu was beneficial for the reaction. In Fig. S23 and S24,† no obvious changes were observed in the structure or morphology of the catalyst after electrolysis, further indicating the stability of the catalyst.

Further study was conducted to reveal the possible reaction pathway. Online differential electrochemical mass spectrometry (DEMS, Fig. S25†) was used to detect the *m/z* signals of 30 and 33, as shown in Fig. 3C, which corresponded to the NO and NH$_2$OH intermediates, respectively, during NO$_3^-$ reduction over 0.6% Cu/TiO$_2$ catalyst. The weak signal of NH$_2$OH indicated that the generated NH$_2$OH spontaneously coupled with cyclohexanone to produce oxime products and could not remain in the bulk electrolyte. Signals of other byproducts were also detected, as shown in Fig. S26.† *In situ* Fourier transform infrared (FTIR) spectroscopy (Fig. S27†) also confirmed the possible involvement of NO and NH$_2$OH signals at 1442 and 1204 cm$^{-1}$ in Fig. 3D on the surface of the 0.6% Cu/TiO$_2$ catalyst during electrosynthesis.[32–34] Additionally, when using D$_2$O as the electrolyte solvent, an obvious peak at 1689 cm$^{-1}$ was observed, as shown in Fig. 3E, indicating the formation of C=N bonds in cyclohexanone oxime molecules that was not observed in H$_2$O solvent because of the interference of O–H bending (1645 cm$^{-1}$).
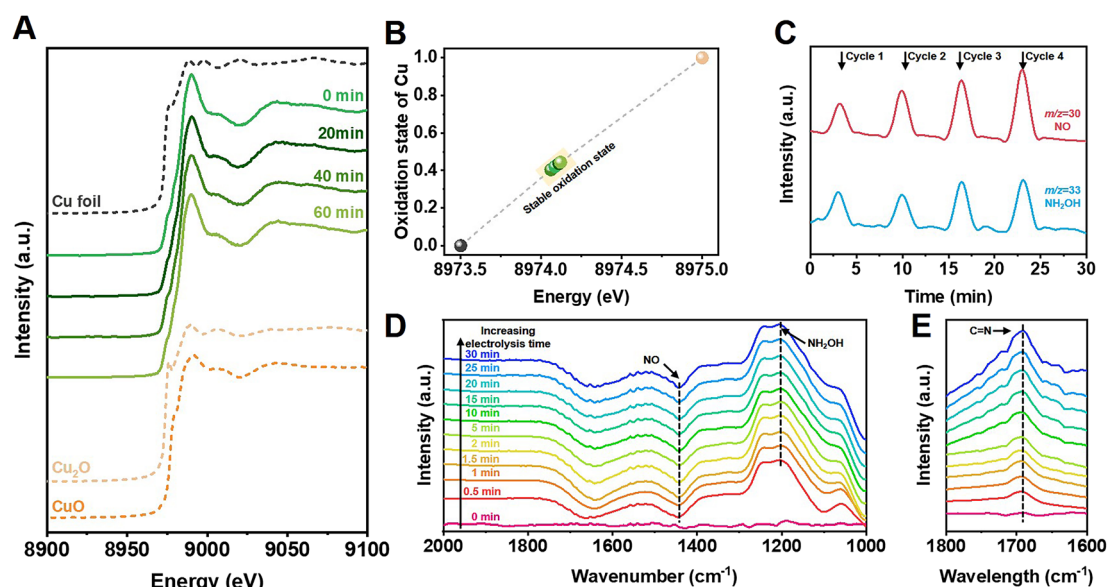


Fig. 3 *In situ* study. (A) XANES spectra at Cu K-edge and (B) Cu oxidation state of 0.6% Cu/TiO$_2$ measured at different electrolysis times during cyclohexanone oxime synthesis. (C) Online DEMS graph of NO and NH$_2$OH intermediates. *In situ* FTIR spectra of electrochemical cyclohexanone synthesis conducted at prolonged electrolysis time on 0.6% Cu/TiO$_2$ in (D) H$_2$O and (E) D$_2$O solvent.

Systematic control experiments were performed to study the reaction pathways of the electrosynthesis of cyclohexanone oxime (Table S1†). No cyclohexanone oxime was detected when there was no cyclohexanone or $NO_3^-$ in the electrolyte (entries 1–3). We also used $NO_2^-$, NO, and $NH_2OH$ as the feedstock, which were formerly identified as the intermediates (entries 4–6). All three entries produced cyclohexanone oxime products. In addition, the C–N coupling between cyclohexanone and $NH_2OH$ was proved to be spontaneous, and occurred without electrolysis (entries 6–7).

The discernible fluctuations in the FE, notably when feeding with NO, were ascribable to the limited solubility of NO gas in aqueous solutions, leading to heightened hydrogen evolution side reactions. Notwithstanding these disparities in the FE, the rate of cyclohexanone oxime formation continued to exhibit a noteworthy level of consistency across all nitrogenous substrates. Therefore, the above results present the possible reaction pathways of $NO_3^-$ to $NH_2OH$ intermediates through $NO_3^- \rightarrow NO_2^- \rightarrow NO \rightarrow NH_2OH$ progression, followed by the nonelectrochemical spontaneous condensation of $NH_2OH$ and cyclohexanone to produce cyclohexanone oxime.

Furthermore, density functional theory (DFT) calculations were conducted to study the reaction pathway (Fig. 4A and S28†). According to high-resolution transmission electron microscopy (HRTEM) images and X-ray diffraction (XRD) patterns, Cu(111) and Cu(111)-$Cu_2O$(110) heterostructures loaded on anatase phase $TiO_2$(101) were used as the catalyst models. A free energy diagram of $NO_3^-$-to-$NH_2OH$ is presented in Fig. 4B. $NO_3^-$ was chemically absorbed on the catalyst to initially form $NO_3^*$ with a decrease in free energy. Then, the deoxygenation and hydrogenation steps were continuously proceeded by $H^+/e^-$ transfer to form $NO_2^*$ and NO*. The conversion of $NO_2^*$ to NOOH* was endergonic and acted as the rate-determining step (RDS), which was consistent with the detection of $NO_2^-$ byproducts during electrolysis. Subsequently, the NO* intermediate was gradually converted to NOH*, NHOH*, and finally to $NH_2OH^*$ under hydrogenation.

The high selectivity of >99.9% is an obvious advantage of cyclohexanone oxime production through an electrocatalysis strategy.[8,35,36] Interestingly, the reduction of cyclohexanone and cyclohexanone oxime were not detected as side reactions because no GC-MS peaks of cyclohexanol or cyclohexylamine appeared in Fig. S6A.† The reduction of excess $NO_x$ substrates as well as a coherent base environment (pH 13.4) of the electrolyte hindered the reduction of organic molecules.[12] Additionally, DFT study revealed the limitation of reduction of cyclohexanone (Fig. 4C) and cyclohexanone oxime (Fig. 4D). The calculated free energy of the absorption of cyclohexanone and cyclohexanone
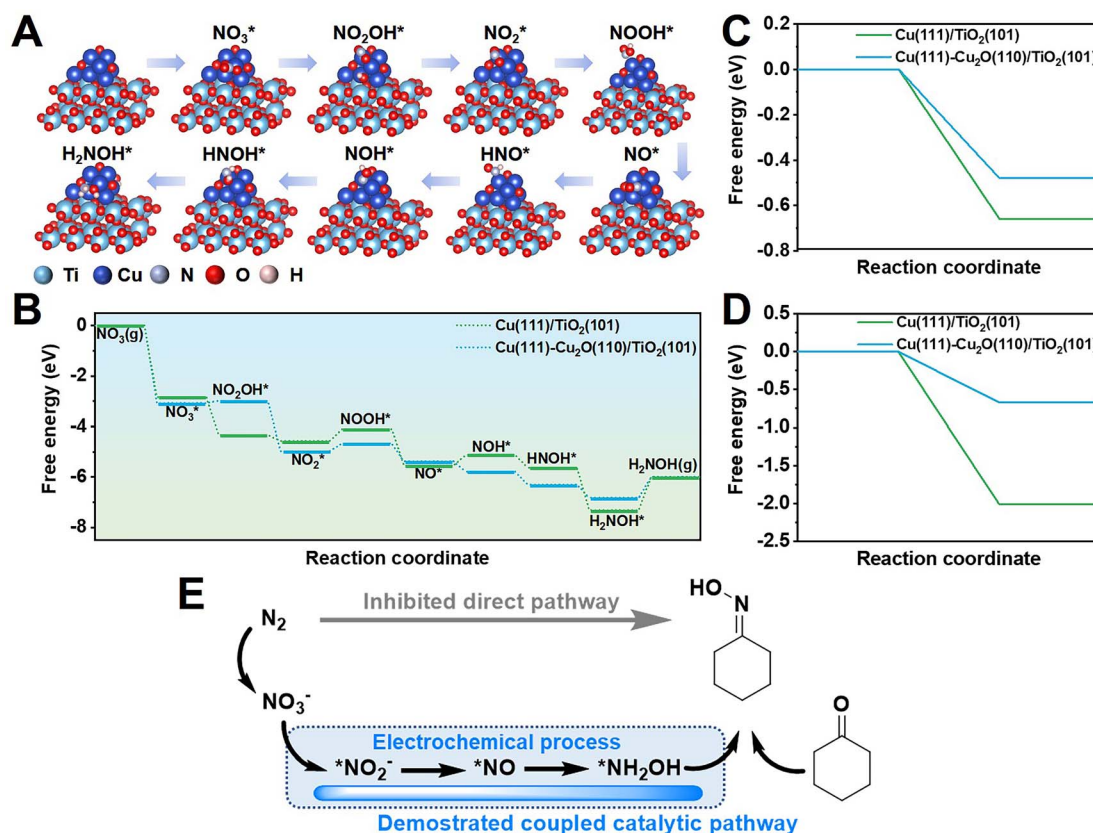


**Fig. 4** Theoretical calculations. (A) Catalytic pathway from $NO_3^-$ to $NH_2OH$ on Cu/$TiO_2$ catalyst according to the optimized configurations with adsorbed intermediates. Cyan, blue, purple, red, and pink balls denote Ti, Cu, N, O, and H, respectively. (B) Gibbs free energy diagrams of $NH_2OH$ generation from $NO_3^-$ on different models. (C) Calculated free energy diagram for (C) cyclohexanone* and (D) cyclohexanone oxime* adsorption on different $TiO_2$-loaded Cu catalytic sites. (E) The proposed pathway of $NH_2OH$ generation and cyclohexanone oxime production.

oxime on Cu(111)-Cu$_2$O(110) models was found to be lower than that on the Cu(111) structure, which implies that the side reactions were hindered during efficient production of cyclohexanone oxime on Cu/TiO$_2$ catalysts. As discussed above, the pathway of cyclohexanone is presented in Fig. 4E. NO$_x$ substrates from air oxidation produced NH$_2$OH through electrocatalysis, followed by its non-electrochemical coupling with cyclohexanone to produce oxime.

The universality of our method was further confirmed by successfully converting a range of aldehydes and ketones in addition to cyclohexanone (*e.g.*, benzaldehyde, acetone, cyclopentanone, and diethyl ketone) into oximes with high FE and selectivity under optimal conditions (Table S2†). This highlights the broad applicability of the electrocatalytic strategy to synthesize oxime, and affirms our proposed reaction pathway.

## Conclusions

We propose a sustainable strategy to efficiently synthesize value-added cyclohexanone oxime using air as a nitrogen source, which includes plasma-assisted air-to-NO$_x$ and co-electrolysis of NO$_x$ and cyclohexanone. The highest performance was provided by 0.6% Cu/TiO$_2$, which produced cyclohexanone at a yield rate of 20.1 mg h$^{-1}$ cm$^{-2}$ and an FE of 51.4%. The selectivity of cyclohexanone oxime was >99.9% on the basis of cyclohexanone. Detailed study indicated that the optimized catalytic activity was ascribed to Cu sites supported on TiO$_2$ with a stable oxidation state.

Further *in situ* characterizations combined with DFT calculations revealed the possible pathway of NO$_3^-$ → NO$_2^-$ → NO → NH$_2$OH → cyclohexanone oxime. Together with transformation routes reported by our group, including the production of phenol using lignin and selective phenol-to-cyclohexanone conversion, this work provides a rational pathway to the synthesis of cyclohexanone oxime with biomass, an air nitrogen source, and green solvent.[37–39] It will also inspire innovative routes to the carbon-natural chemical manufacturing of industrially important fine C–N chemicals from renewable carbon sources and nitrogen using clean energy.

## Data availability

All experimental data is available in the ESI.†

## Author contributions

S. H. J., X. F. S., and B. X. H. proposed the project, designed the experiments, and wrote the manuscript. S. H. J. performed all the experiments. X. X. T., L. M. W., and X. D. M. performed the analysis of the experimental data. L. B. Z., J. Q. F., L. X., and X. N. S. conducted portions of the characterization study. Q. G. Z. and X. C. K. participated in discussions. X. F. S. and B. X. H. supervised the entire project.

## Conflicts of interest

There are no conflicts to declare.

## References

1 J. W. Erisman, M. A. Sutton, J. Galloway, Z. Klimont and W. Winiwarter, *Nat. Geosci.*, 2008, **1**, 636–639.

2 M. A. Tarselli, *Nat. Chem.*, 2012, **4**, 686.

3 J. N. Galloway, A. R. Townsend, J. W. Erisman, M. Bekunda, Z. Cai, J. R. Freney, L. A. Martinelli, S. P. Seitzinger and M. A. Sutton, *Science*, 2008, **320**, 889–892.

4 J. G. Chen, R. M. Crooks, L. C. Seefeldt, K. L. Bren, R. M. Bullock, M. Y. Darensbourg, P. L. Holland, B. Hoffman, M. J. Janik, A. K. Jones, M. G. Kanatzidis, P. King, K. M. Lancaster, S. V. Lymar, P. Pfromm, W. F. Schneider and R. R. Schrock, *Science*, 2018, **360**, eaar6611.

5 S. L. Foster, S. I. P. Bakovic, R. D. Duda, S. Maheshwari, R. D. Milton, S. D. Minteer, M. J. Janik, J. N. Renner and L. F. Greenlee, *Nat. Catal.*, 2018, **1**, 490–500.

6 X. Chen, S. Song, H. Li, G. Gözaydın and N. Yan, *Acc. Chem. Res.*, 2021, **54**, 1711–1722.

7 M. Hua, J. Song, X. Huang, H. Liu, H. Fan, W. Wang, Z. He, Z. Liu and B. Han, *Angew. Chem., Int. Ed.*, 2021, **60**, 21479–21485.

8 R. J. Lewis, K. Ueura, X. Liu, Y. Fukuta, T. E. Davies, D. J. Morgan, L. Chen, J. Qi, J. Singleton, J. K. Edwards, S. J. Freakley, C. J. Kiely, Y. Yamamoto and G. J. Hutchings, *Science*, 2022, **376**, 615–620.

9 R. Xia, S. Overa and F. Jiao, *JACS Au*, 2022, **2**, 1054–1070.

10 H. Iriawan, S. Z. Andersen, X. Zhang, B. M. Comer, J. Barrio, P. Chen, A. J. Medford, I. E. L. Stephens, I. Chorkendorff and Y. Shao-Horn, *Nat. Rev. Methods Primers*, 2021, **1**, 56.

11 M. He, Y. Sun and B. Han, *Angew. Chem., Int. Ed.*, 2022, **61**, e202112835.

12 Z.-J. Lv, J. Wei, W.-X. Zhang, P. Chen, D. Deng, Z.-J. Shi and Z. Xi, *Natl. Sci. Rev.*, 2020, **7**, 1564–1583.

13 R. Xu, D.-H. Si, S.-S. Zhao, Q.-J. Wu, X.-S. Wang, T.-F. Liu, H. Zhao, R. Cao and Y.-B. Huang, *J. Am. Chem. Soc.*, 2023, **145**, 8261–8270.

14 D.-L. Meng, M.-D. Zhang, D.-H. Si, M.-J. Mao, Y. Hou, Y.-B. Huang and R. Cao, *Angew. Chem., Int. Ed.*, 2021, **60**, 25485–25492.

15 B. H. R. Suryanto, K. Matuszek, J. Choi, R. Y. Hodgetts, H.-L. Du, J. M. Bakker, C. S. M. Kang, P. V. Cherepanov, A. N. Simonov and D. R. MacFarlane, *Science*, 2021, **372**, 1187–1191.

16 H.-L. Du, M. Chatti, R. Y. Hodgetts, P. V. Cherepanov, C. K. Nguyen, K. Matuszek, D. R. MacFarlane and A. N. Simonov, *Nature*, 2022, **609**, 722–727.

17 P. Garrido-Barros, J. Derosa, M. J. Chalkley and J. C. Peters, *Nature*, 2022, **609**, 71–76.

18 C. Chen, X. Zhu, X. Wen, Y. Zhou, L. Zhou, H. Li, L. Tao, Q. Li, S. Du, T. Liu, D. Yan, C. Xie, Y. Zou, Y. Wang, R. Chen, J. Huo, Y. Li, J. Cheng, H. Su, X. Zhao, W. Cheng, Q. Liu, H. Lin, J. Luo, J. Chen, M. Dong, K. Cheng, C. Li and S. Wang, *Nat. Chem.*, 2020, **12**, 717–724.

19 S. Jia, X. Ma, X. Sun and B. Han, *CCS Chem.*, 2022, **4**, 3213–3229.

20 L. Li, C. Tang, X. Cui, Y. Zheng, X. Wang, H. Xu, S. Zhang, T. Shao, K. Davey and S.-Z. Qiao, *Angew. Chem., Int. Ed.*, 2021, **60**, 14131–14137.

21 Y. Ren, C. Yu, L. Wang, X. Tan, Z. Wang, Q. Wei, Y. Zhang and J. Qiu, *J. Am. Chem. Soc.*, 2022, **144**, 10193–10200.

22 Y. Wu, Z. Jiang, Z. Lin, Y. Liang and H. Wang, *Nat. Sustain.*, 2021, **4**, 725–730.

23 J. Li, Y. Zhang, K. Kuruvinashetti and N. Kornienko, *Nat. Rev. Chem*, 2022, **6**, 303–319.

24 G. Dahlhoff, J. P. M. Niederer and W. F. Hoelderich, *Catal. Rev.*, 2001, **43**, 381–441.

25 R. Mokaya and M. Poliakoff, *Nature*, 2005, **437**, 1243–1244.

26 J. M. Thomas and R. Raja, *Proc. Natl. Acad. Sci. U. S. A.*, 2005, **102**, 13732–13736.

27 Y. Fu, S. Wang, Y. Wang, P. Wei, J. Shao, T. Liu, G. Wang and X. Bao, *Angew. Chem., Int. Ed.*, 2023, **62**, e202303327.

28 L. Wu, J. Feng, L. Zhang, S. Jia, X. Song, Q. Zhu, X. Kang, X. Xing, X. Sun and B. Han, *Angew. Chem., Int. Ed.*, 2023, **62**, e202307952.

29 Q. Gao, B. Yao, H. S. Pillai, W. Zang, X. Han, Y. Liu, S.-W. Yu, Z. Yan, B. Min, S. Zhang, H. Zhou, L. Ma, H. Xin, Q. He and H. Zhu, *Nat. Synth.*, 2023, **2**, 624–634.

30 S. Zhang, J. Wu, M. Zheng, X. Jin, Z. Shen, Z. Li, Y. Wang, Q. Wang, X. Wang, H. Wei, J. Zhang, P. Wang, S. Zhang, L. Yu, L. Dong, Q. Zhu, H. Zhang and J. Lu, *Nat. Commun.*, 2023, **14**, 3634.

31 X. Li, Y. Chen, X. Zhan, Y. Xu, L. Hao, L. Xu, X. Li, M. Umer, X. Tan, B. Han, A. W. Robertson and Z. Sun, *The Innovation Materials*, 2023, **1**, 100014.

32 M. Duca, M. C. Figueiredo, V. Climent, P. Rodriguez, J. M. Feliu and M. T. M. Koper, *J. Am. Chem. Soc.*, 2011, **133**, 10928–10939.

33 E. Pérez-Gallent, M. C. Figueiredo, I. Katsounaros and M. T. M. Koper, *Electrochim. Acta*, 2017, **227**, 77–84.

34 Y. Yao, S. Zhu, H. Wang, H. Li and M. Shao, *J. Am. Chem. Soc.*, 2018, **140**, 1496–1501.

35 Y. Wu, J. Zhao, C. Wang, T. Li, B.-H. Zhao, Z. Song, C. Liu and B. Zhang, *Nat. Commun.*, 2023, **14**, 3057.

36 Y. Wu, W. Chen, Y. Jiang, Y. Xu, B. Zhou, L. Xu, C. Xie, M. Yang, M. Qiu, D. Wang, Q. Liu, Q. Liu, S. Wang and Y. Zou, *Angew. Chem., Int. Ed.*, 2023, **62**, e202305491.

37 H. Liu, T. Jiang, B. Han, S. Liang and Y. Zhou, *Science*, 2009, **326**, 1250–1252.

38 R. Wu, Q. Meng, J. Yan, H. Liu, Q. Zhu, L. Zheng, J. Zhang and B. Han, *J. Am. Chem. Soc.*, 2022, **144**, 1556–1571.

39 J. Yan, Q. Meng, X. Shen, B. Chen, Y. Sun, J. Xiang, H. Liu and B. Han, *Sci. Adv.*, 2020, **6**, eabd1951.